Journal of Molecular Structure 987 (2011) 106–118

Contents lists available at ScienceDirect

Journal of Molecular Structure

journal homepage: www.elsevier.com/locate/molstruc

X-ray, DFT, FTIR and NMR structural study of 2,3-dihydro-2-(R-phenylacylidene)-1,3,3-trimethyl-1*H*-indole

Oscar F. Vázquez-Vuelvas [a,*], Julia V. Hernández-Madrigal [a], Rubén Gaviño [b], Mikhail A. Tlenkopatchev [c], David Morales-Morales [b], Juan M. Germán-Acacio [b], Zeferino Gomez-Sandoval [a], Cesar Garcias-Morales [d], Armando Ariza-Castolo [d], Armando Pineda-Contreras [a]

[a] *Facultad de Ciencias Químicas, Universidad de Colima, km 9 Carr. Colima-Coquimatlán s/n, 28400 Coquimatlán, Colima, Mexico*
[b] *Instituto de Química, Universidad Nacional Autónoma de México, Circuito Exterior, Ciudad Universitaria, México D.F. 04510, Mexico*
[c] *Instituto de Investigaciones en Materiales, Universidad Nacional Autónoma de México, Circuito Exterior, Ciudad Universitaria, México D.F. 04510, Mexico*
[d] *Centro de Investigación y de Estudios Avanzados del I.P.N., Apdo. Postal 14-740, México D.F. 07000, Mexico*

ARTICLE INFO

Article history:
Received 12 June 2010
Received in revised form 6 December 2010
Accepted 6 December 2010
Available online 15 December 2010

Keywords:
Fischer base
X-ray diffraction
Enaminoketone
FTIR
DFT
NMR

ABSTRACT

Fischer base derivatives are widely used as precursor in the formation of different chemical switches. Besides, in the presence of acyl chlorides, indole enaminoketone derivatives can be prepared. 2,3-Dihydro-2-(R-phenylacylidene)-1,3,3-trimethyl-1*H*-indole, R = 4-NO_2, 3,5-$(NO_2)_2$ and 4-OCH_3, have been characterized previously but only by ^{1}H NMR, thus further characterization was performed by FTIR, ^{13}C NMR and when suitable crystals were obtained by single crystal X-ray diffraction analyses. The structures of the three molecules were additionally analyzed by DFT methods, B3LYP and PW91 functionals, using 6-311G(d,p) basis set. The optimized structures obtained were compared with those determined by crystallographic data. The probable assignments of the anharmonic experimental solid state vibrational frequencies for these molecules have been also made based on the calculated harmonic frequencies in vacuum at the same level of theory for the optimized structures. Correlations between experimental chemical shifts and GIAO calculated magnetic isotropic shielding constants with B3LYP and PW91 functionals using the 6-311++G(3df,3pd) basis set are also reported.

1. Introduction

The Fischer base, 2,3-dihydro-1*H*-1,3,3-trimethyl-2-methyleneindole and some derivatives have been widely used in organic synthesis for the preparation of different types of chemical switches [1]. Products with different photochromic and thermochromic properties have been reported due to their potential practical application in optoelectronics, molecular information devices and as organic electroluminescence materials [2–4]. Further applications include the use of different derivatives in the field of dyes [5]. The spiropyran and spirooxazine derivatives of the Fischer base have acquired in recent years industrial relevance in areas such as: the production of polymer-based photochromic lenses, colorants for textiles and surface coatings, including photochromic inks and aesthetic uses [6,7] due to their photochemical properties. These products can be conveniently prepared from indole enaminoketones derivatives and this synthetic procedure is not limited to the synthesis of spiropyrans and spirooxazines [8], but also for the production of acetylenic products via indole enaminoketone fragmentation [9–11].

The synthesis of Fischer base enaminoketone derivatives with different acyl-substituted enamino carbonyl derivatives, as well as their characterization by NMR and FTIR spectroscopies have been previously studied in order to define conformational and configurational structures [12].

Additionally, the synthesis and analysis in solution by ^{1}H NMR spectroscopy of several enaminoketones has also been reported [13]. However, despite the great interest in Fischer base derivatives, indole enaminoketones have been poorly studied and little is known about their structures. The potential importance of these species as precursors of chemical switches and arylacetylenes provides further motivation for the unambiguous structure determination of these compounds.

On this opportunity, we would like to report the full and unequivocal characterization and solid structural studies of different enaminoketone derivatives namely 2,3-dihydro-2-(R-phenylacylidene)-1,3,3-trimethyl-1*H*-indole (**1c**, R = 4-NO_2, **2c**, 3,5-$(NO_2)_2$, **3c**, 4-OCH_3), (Fig. 1). In addition, DFT methods using the hybrid B3LYP correlation and PW91 exchange-correlation functionals were employed for the determination of calculated geometric

* Corresponding author. Tel.: +52 312 316 11 63.
E-mail address: oscar_vazquez@ucol.mx (O.F. Vázquez-Vuelvas).

0022-2860/$ - see front matter © 2010 Elsevier B.V. All rights reserved.
doi:10.1016/j.molstruc.2010.12.001

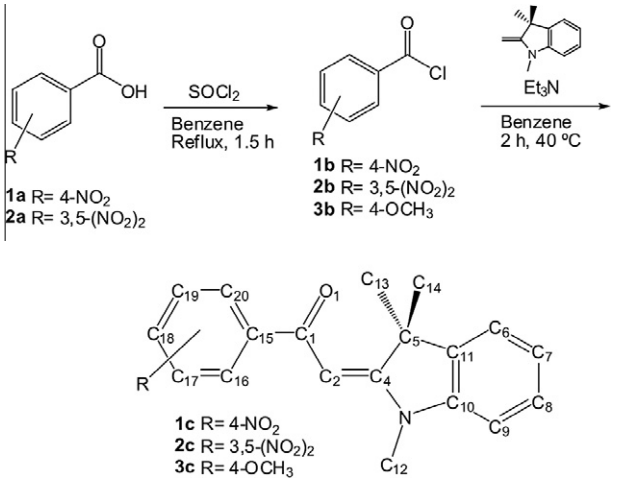

Fig. 1. Synthetic route and atom numbering of indole enaminoketones **1c**, **2c** and **3c**. Hydrogen atom symbols have been omitted for clarity.

parameters, vibrational frequencies and chemical shifts, these results were analyzed and compared with those obtained from experimental results.

2. Experimental

2.1. (E)-2,3-Dihydro-2-(4-nitrophenylacylidene)-1,3,3-trimethyl-1H-indole (*1c*)

The synthesis of this compound has been previously reported [13,14]. In the present work, to a solution of **1a** (10 g, 59.84 mmol) in 72 ml of dry benzene thionyl chloride (14.24 g, 119.68 mmol) was added, the mixture was heated at reflux for 1.5 h. After the prescribed reaction time, the reaction mixture was allowed to cool down to room temperature, and both the solvent and excess of thionyl chloride evaporated; for its complete removal, 30 ml of petroleum ether was added and eliminated under a vacuum. A solution of **1b** in 50 ml of dry benzene was added to a mixture of the Fischer base 2,3-dihydro-1*H*-1,3,3-trimethyl-2-methyleneindole (10.36 g, 59.84 mmol) and triethylamine (7.26 g, 71.78 mmol) in 100 ml of dry benzene. The mixture was maintained at 40 °C for 2 h, and then allowed to stand overnight at room temperature. The resulting precipitate was filtered and washed with water and isopropyl alcohol. The product was purified by column chromatography using chloroform as eluent. The yield was 15.24 g (79%); m.p.: 194–196 °C. Literature [13]: 193–196 °C.

2.2. (E)-2,3-Dihydro-2-(3,5-dinitrophenylacylidene)-1,3,3-trimethyl-1H-indole (*2c*)

Compound **2c** was synthesized by the same procedure as that described for compound **1c**. Yield 65%; m.p. of 217–221 °C. Literature [13]: 215–220 °C.

2.3. (E)-2,3-Dihydro-2-(4-methoxyphenylacylidene)-1,3,3-trimethyl-1H-indole (*3c*)

Compound **3c** from **3b** was synthesized following the same procedure as that described above for compound **1c**. Yield 59%; m.p.: 151–153 °C. Literature [13]: 148–150 °C.

The infrared spectra of the three compounds were recorded in a Varian 3100 FT-IR Excalibur Series spectrometer in the range of 4000–400 cm^{-1}. The solid substances were analyzed with an ATR device, which was evacuated to avoid water and CO_2 absorptions, at a 4 cm^{-1} resolution with 32 scans. ^1H and ^{13}C NMR for compounds **1c** and **2c** were recorded in solution with $CDCl_3$ and TMS in a Varian 300 Unity Inova spectrometer at 300 MHz for ^1H and 75 MHz for ^{13}C. Compound **3c** was recorded in a Bruker Avance III spectrometer at 400 MHz for ^1H and 100 MHz for ^{13}C.

Suitable crystals for X-ray diffraction were obtained from its toluene solution by slow evaporation. Crystals of **1c** and **2c** were mounted in random orientation on glass fibers. The X-ray intensity data were measured at 298 K and 123 K, for **1c** and **2c**, respectively, on a Bruker SMART APEX CCD-based three-circle X-ray diffractometer system using graphite mono-chromated Mo Kα radiation (λ = 0.71073 Å). The crystal structures were solved by direct methods and refined using SHELXS-97 and SHELXL-97 crystallographic software packages [15–17]. All non-hydrogen atoms were refined anisotropically using reflections $I > 2\sigma(I)$. Hydrogen atoms were located in ideal positions. Geometric calculations were done using PLATON [18]. Crystal of **3c** was supported on a glass fiber. The diffraction data were collected in an Enraf–Nonius CCD with Mo Kα radiation (λ = 0.71073 Å) with area detector. The software used for data collection, indexing reflections, and parameter recording for the lattice was CAD4 EXPRESS. Data reduction was performed using WinGX [19] and SHELXS-97 crystallographic software packages [17]. Molecular graphics, visualization and analysis of the three crystal structures were prepared using MERCURY [20].

The details of the structure determination are listed in Table 1, selected bond lengths (Å), selected bond and dihedral angles (°) are listed in Table 3. The atom numbering of crystal structures **1c**, **2c** and **3c** are depicted in Figs. 3a, 4a and 5a, respectively. CCDC 772890–772892 contains the supplementary crystallographic data for this paper. These data can be obtained free of charge via http://www.ccdc.cam.ac.uk/conts/retrieving.html (or from the Cambridge Crystallographic Data Centre, 12, Union Road, Cambridge CB2 1EZ, UK; fax: +44 1223 336033).

2.4. Computational details

The calculations were performed using the Gaussian 03 program package [21]. The geometries of all structures were fully optimized with two different functionals, B3LYP [22,23] and PW91 [24] in conjunction with 6-311G(d,p) basis set without any symmetry restrictions. The calculations were carried out based on crystallographic data from the three enaminoketone molecules **1c**, **2c** and **3c**. The minimum energy was verified by calculating the vibrational frequencies for the optimized structures at the same level of theory and compared with experimental FTIR data. Magnetic shielding tensors were computed using the standard GIAO (Gauge-Independent Atomic Orbital) DFT method as implemented in the Gaussian 03 program package employing two different functionals, B3LYP and PW91 using the 6-311++G(3df,3pd) basis set. The SCF convergence criterion for the compound **2c** was set to 10^{-7} on the density matrix and to 10^{-5} au on the r.m.s. force for both functionals due to termination failures in the calculating process. In order to get visualization of the shape of the different molecular vibrational modes and the corresponding assignment of the calculated wavenumbers, the visualization program for working with quantum chemistry computations Chemcraft software was used [25].

3. Results and discussion

3.1. Quantum chemical calculations

To support the experimental results, an extension of the study was done by theoretical calculations. Regarding indole enaminoketones can exist in two conformations, *s-cis* and *s-trans*, and with allowance for geometrical isomerism relative to exocyclic C=C

Table 1
Structure refinement data for crystals of **1c**, **2c** and **3c** compounds.

	1c	**2c**	**3c**
Empirical formula	$C_{19}H_{18}N_2O_3$	$C_{19}H_{17}N_3O_5$	$C_{20}H_{21}NO_2$
Formula weight	322.35	367.36	307.38
Temperature (K)	298(2)	123(2)	293(2)
Wavelength (Å)	0.71073	0.71073	0.71073
Crystal system	Triclinic	Triclinic	Monoclinic
Space group	*P*-1	*P*-1	$P\,2_1/a$
a (Å)	8.5784(13)	6.9082(9)	8.564
b (Å)	9.0870(13)	7.8601(11)	15.345
c (Å)	11.1379(16)	15.578(2)	12.936
α (°)	79.926(2)	99.232(3)	90
β (°)	78.848(2)	91.361(3)	90.940
γ (°)	86.990(2)	93.420(3)	90
Volume (Å^3)	838.5(2)	832.97(19)	1699.75
Z	2	2	4
Density (calculated) (Mg/m^3)	1.277	1.465	1.201
Absorption coefficient (mm^{-1})	0.087	0.108	0.077
F(0 0 0)	340	384	656
Crystal size (mm)	0.372 × 0.164 × 0.126	0.388 × 0.212 × 0.104	0.4 × 0.4 × 0.4
Theta range for data collection (°)	1.89–5.37	2.63–5.45	3.1–7.71
Index ranges	$-10 \leqslant h \leqslant 10$	$-8 \leqslant h \leqslant 8$	$-8 \leqslant h \leqslant 8$
	$-10 \leqslant k \leqslant 10$	$-9 \leqslant k \leqslant 9$	$-9 \leqslant k \leqslant 9$
	$-13 \leqslant l \leqslant 13$	$0 \leqslant l \leqslant 18$	$0 \leqslant l \leqslant 18$
Reflections collected	10,847	3076	12,007
Independent reflections	3076 [*R*(int) = 0.0313]	3076 [*R*(int) = 0.0397]	3444 [*R*(int) = 0.048]
Absorption correction	Semi-empirical from equivalents	Semi-empirical from equivalents	None
Max. and min. transmission	0.9898 and 0.9726	0.989 and 0.870	0.97
Refinement method	Full-matrix least-squares on F^2	Full-matrix least-squares on F^2	Full-matrix least-squares on F^2
Data/restraints/parameters	3076/84/248	3076/0/248	3444/0/293
Goodness-of-fit on F^2	1.026	1.04	1.036
Final *R* indices [$I > 2\sigma(I)$]	R_1 = 0.0461, wR_2 = 0.1150	R_1 = 0.0409, wR_2 = 0.0906	R_1 = 0.0605 wR_2 = 0.1354
R indices (all data)	R_1 = 0.0655, wR_2 = 0.1271	R_1 = 0.0479, wR_2 = 0.0941	R_1 = 0.1002 wR_2 = 0.1606
Largest diff. peak and hole	0.213 and −0.178 e Å^{-3}	0.229 and −0.173 e Å^{-3}	0.15 and −0.15 e Å^{-3}

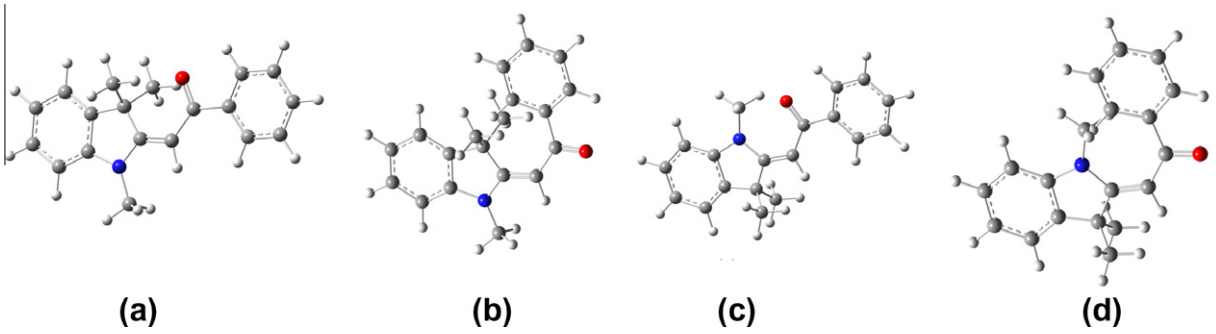

Fig. 2. Analyzed structures of the enaminoketones, (a) (*E*) *s-cis*, (b) (*E*) *s-trans*, (c) (*Z*) *s-cis*, and (d) (*Z*) *s-trans*.

bond, there are four possible conformations to investigate. The general structures of the four studied compounds are shown in Fig. 2.

Taking into account the DFT calculations, the lowest-energy isomers were determined. The total energies *E*, relative ΔE energies and relative Gibbs free energies ΔG of the isomers at B3LYP and PW91 levels are listed in Table 2. Calculated energies confirm that the most stable structures are those with *E* configuration and *s-cis* conformation for **1c**, **2c** and **3c** compounds.

The data of calculated energy in Table 2 show that the lowest values correspond to the energies calculated with B3LYP. The energy difference for (*Z*) *s-cis* structures was in the range of 1.67 and 1.90 kcal/mol for the three compounds with respect to the (*E*) *s-cis* isomer. The difference showed in total energy by compound **3c** in the (*Z*) *s-trans* conformation, is high in comparison with those for similar conformations in **1c** and **2c** due to **3c** presenting one imaginary frequency attributable to the highly steric hindrance of this unstable isomer.

In the subsequent, the discussion will be referred to the energetically most stable (*E*) *s-cis* structures of **1c**, **2c** and **3c** compounds.

3.2. Crystal structures

The enaminoketones **1c** and **2c** crystallized in a triclinic space group $P\bar{1}$, and **3c** crystallized in a monoclinic space group $P2_1/a$. In three cases the conformation observed for the molecules is (*E*) *s-cis*. Selected bond distances and angles are listed on Table 3. For the three structures, bond distances and angles of the indole moiety are similar to those reported for other indole derivatives [4,26]. The bond distances of N(3)—C(10) goes from 1.405(3) Å to 1.414(3) Å, denoting a longer distance than that corresponding to a single Nsp^3—Csp^2 bond of an indole. The same observation occurs with the N(3)—C(4) bonds, with distances ranging from 1.354(3) Å to 1.369(2) Å [4,27]. In addition, the formally double C(2)—C(4) and C(1)—O(1) bonds show 1.367(3)—1.379(3) Å, and 1.236(3)—

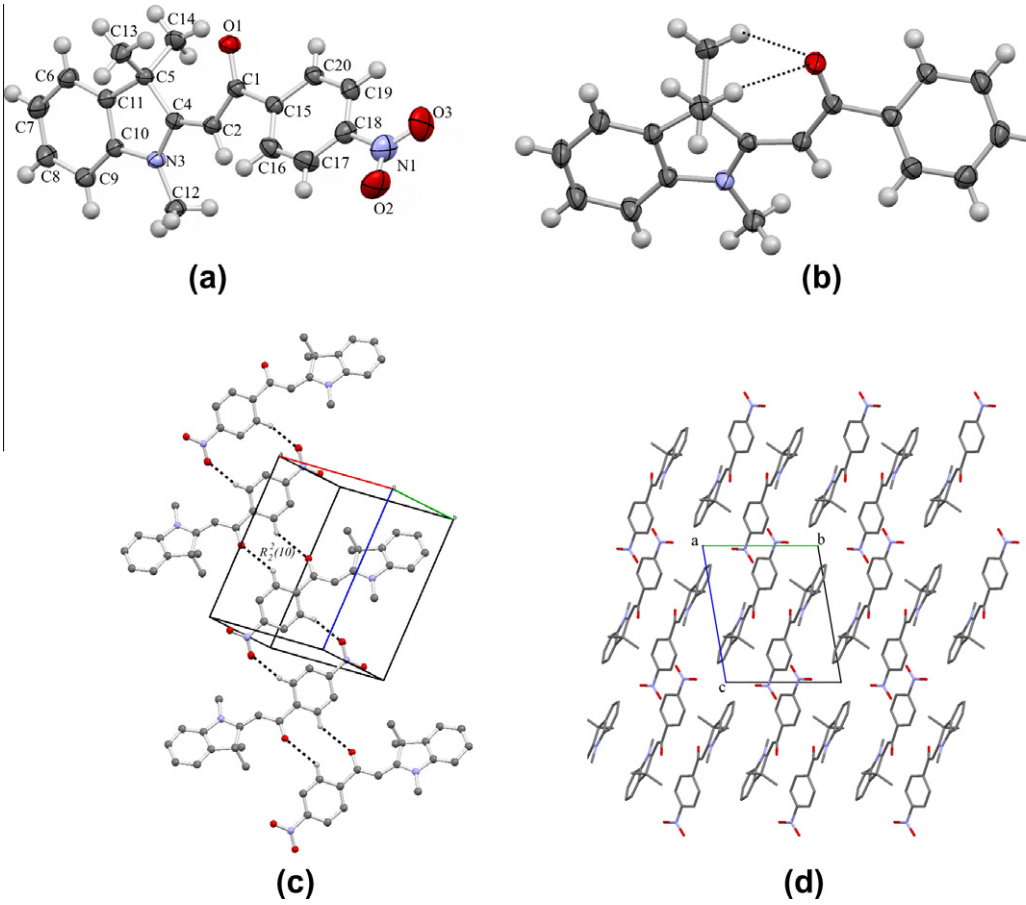

Fig. 3. (a) Molecular structure of **1c** at 30% of probability level and atom numbering. (b) Intramolecular hydrogen contacts, view along C(13)—C(5) bond. (c) Visualization of C—H···O interactions as well as the intermolecular ring and chain formed, hydrogen atoms were omitted for clarity. (d) Packing pattern view along *a* axis, hydrogen atoms were omitted for clarity.

1.243(3) Å bond distances respectively; the average of these distances being slightly longer than those reported for similar derivatives [28]. Conversely, the C(2)—C(1) bonds are shorter than expected for a typical C—C single bond, with bond distances between 1.424 (3) Å and 1.444(2) Å. These values can be attributed to conjugative delocalization of the lone pair of the nitrogen of the amino group with the α,β-unsaturated carbonyl moiety and thus the amino group exhibits a planar geometry (Table 3) [29]. In all cases, the molecules present a virtually planar conformation at the indole moiety, this being showed by the value of their interplanar angles of the adjacent rings [(C(6)—C(11) and N(3)—C(4)—C(5)—C(10)—C(11)] of almost 1°. The exocyclic carbon chain in compound **1c** presents a minor distortion of the plane and this fact being reflected in the dihedral angle C(1)—C(2)—C(4)—C(5), which denotes a tendency to twist around the formal double bond with an angle of −3.5(3)°. In addition, the dihedral angle O(1)—C(1)—C(2)—C(4) in **1c** is −6.3(3)°, whereas in **2c** and **3c** this angles are 5.8(4)° and 4.6(4)° respectively, showing an inverted rotation of the carbonyl group in **1c** with respect to the C=C bond (Table 3). For the same compound the phenyl ring C(15)—C(20), is slightly twisted away from the carbonyl plane with a torsion angle O(1)—C(1)—C(15)—C(20) of −32.1(2)° for **1c**, −16.4(3)° in **2c** and by an intermediate value of 24.8(3)° in **3c**.

The nitro groups in **1c** and **2c** are rotated from the plane of the adjacent aryl ring. In compound **1c**, the nitro is twisted away from the plane of C(15)—C(20) ring with −7(1)° denoted by the torsion angle C(17)—C(18)—N(1)—O(2). Compound **2c** presents an interplanar spacing with the torsion angle formed by O(1)—N(1)—C(18)—C(17) of −13.6(3)° and C(18)—C(19)—N(2)—O(4) of −15.8(3)°. The methoxy group of the crystal **3c** has almost the same benzene ring plane, the torsion angle is C(21)—O(2)—C(18)—C(17) = 2.9(3)°.

The geometric parameters associated with intra and intermolecular D—H···A interactions are listed in Table 4. Non classic neither intra nor intermolecular hydrogen bonds are present. However, weak C—H···O contacts, depicted in the supramolecular assembly govern the intermolecular crystal packing. The main interactions found in **1c** and **2c**, are of the type C—H···O of the nitro group. Compound **3c** presents short contacts of type C—H···O involving the carbonyl and the methoxy groups (Table 4). The aforementioned contacts determine the stacking mode of the molecules in the solid state due to the high coplanar difference of the two-side aromatic rings and their substituents. Since the coplanar angle between the rings is 38.29°, 17.61° and 31.06 for **1c**, **2c** and **3c** respectively, no short face-to-face π–π stacking interactions are observed in the crystal packing of **1c** and **2c**, but they are present in **3c**, exhibiting a C—H···O contact motif in a similar edge-to-face fashion involving the methoxy group. For all the nitro groups involved in short contacts, the C—H···O=N and C···O=N distances are shorter than the mean values reported in the literature [30]. Moreover, the not very basic nitro group acts as a C—H···O acceptor in the crystal structures of our unsaturated compounds, due to the enhanced acceptor ability of the nitro group, this probably being due to conjugation and cooperativity effects [31].

The structures of the three compounds exhibit C—H···O intermolecular contacts in a bifurcated fashion with C(13) and C(14)

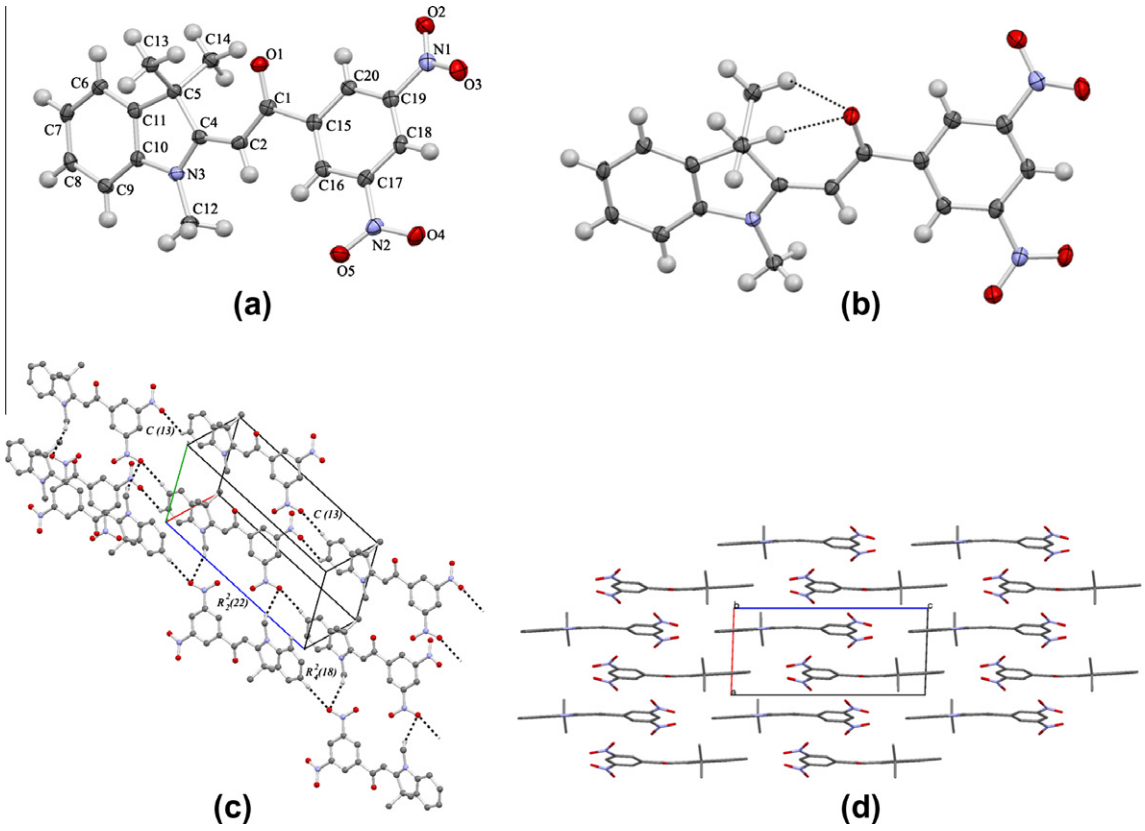

Fig. 4. (a) Molecular structure of **2c** at 50% of probability level and atom numbering. (b) Intramolecular hydrogen bonds, view along C(13)—C(5) bond. (c) Visualization of C—H···O interactions as well as the intermolecular ring and chain formed, hydrogen atoms were omitted for clarity. (d) Packing patter view along *a* axis, hydrogen atoms were omitted for clarity.

Table 2
Calculated B3LYP/6-311G(d,p) and PW91/6-311G(d,p) total *E*, Δ*E* and Δ*G* energies (kcal/mol) of the enaminoketone isomers.

Compound	Structure	B3LYP			PW91		
		E	Δ*E*	Δ*G*	*E*	Δ*E*	Δ*G*
1c	(*E*) *s-cis*	−1070.216421	0.00	0.00	−1069.846275	0.00	0.00
	(*Z*) *s-cis*	−1070.213767	1.67	1.64	−1069.843568	1.70	2.14
	(*Z*) *s-trans*	−1070.204420	7.53	7.63	−1069.835218	6.94	7.72
	(*E*) *s-trans*	−1070.199097	10.87	10.45	−1069.830098	10.15	10.43
2c	(*E*) *s-cis*	−1274.768228	0.00	0.00	−1274.370640	0.00	0.00
	(*Z*) *s-cis*	−1274.765389	1.78	2.03	−1274.367610	1.90	1.77
	(*Z*) *s-trans*	−1274.755042	8.27	8.59	−1274.353537	7.68	7.73
	(*E*) *s-trans*	−1274.749926	11.48	11.51	−1274.353537	10.73	10.53
3c	(*E*) *s-cis*	−980.214913	0.00	0.00	−979.836457	0.00	0.00
	(*Z*) *s-cis*	−980.212174	1.72	1.51	−979.833633	1.77	1.80
	(*Z*) *s-trans*	−980.186022[a]	18.13	9.72	−979.809834[a]	16.71	11.44
	(*E*) *s-trans*	−980.199005	9.98	9.63	−979.821320	9.50	9.82

[a] There is one imaginary frequency for the structure, the local minimum has not been found.

as the donor atoms and the oxygen of carbonyl group O(1) as the acceptor (Figs. 3b, 4b and 5b; Table 4). In **1c**, the supramolecular structure presents an arrangement antiparallel in a head-to-tail stacking mode especially favored by the formation of a homodimer determined by the C—H···O=C interactions. These are formed with the donor C(20) atom at (*x*, *y*, *z*) and O(1) atom at (−*x*, 1 − *y*, 1 − *z*), and by inversion, it is formed a ring R_2^2 (10) in graph notation [32] (Fig. 3c; Table 4). Additionally, a C—H···O contact was observed with the N(1B)—O(2B)—O(3B) atoms, whose occupancy exceeded the nitro site. The contact is formed with the C(16) atom at (*x*, *y*, *z*) as the donor and O(2B) at (1 − *x*, 1 − *y*, 2 − *z*) as the acceptor of the interaction.

For compound **2c**, the supramolecular assembly presents a homodimer formed with the presence of C—H···O donor atom C(12) at (*x*, *y*, *z*), interacting with the nitro O(3) atom in the molecule at (−*x*, −*y*, 1 − *z*), and by inversion it forms a ring R_2^2 (22) (Fig. 4c; Table 4). At the same time, acceptor atom O(3) at (*x*, *y*, *z*) is engaged with donor atom C(7) at (*x*, *y*, 1 + *z*) to form a suitable hydrogen contact, and therefore propagation by inversion forms another ring R_4^2 (18). Additionally, the donor C(8) atom at (*x*, *y*, *z*) interacts with the acceptor O(4) atom at (*x*, −1 + *y*, −1 + *z*) to form the chains *C*(*13*), as well as the C(7)—H(7)···O(3) hydrogen contact form the chain C(*14*) by motif propagation, consequently the formation of layers of the hydrogen contacts interlinked ribbon chains.

Table 3
Experimental and calculated data with B3LYP/6-311G(d,p) and PW91/6-311G(d,p) of bond lengths (Å), bond angles and selected dihedral angles (°) for **1c**, **2c** and **3c**.

Parameter	X-ray	B3LYP	PW91	X-ray	B3LYP	PW91	X-ray	B3LYP	PW91
Bond lengths	**1c**			**2c**			**3c**		
C(1)—O(1)	1.243(3)	1.231	1.243	1.237(2)	1.232	1.244	1.236(3)	1.233	1.246
C(1)—C(2)	1.424(3)	1.442	1.442	1.432(2)	1.448	1.448	1.444(2)	1.456	1.455
C(1)—C15	1.525(3)	1.524	1.524	1.508(2)	1.518	1.518	1.502(3)	1.506	1.506
C(2)—C(4)	1.379(3)	1.378	1.384	1.368(2)	1.375	1.382	1.367(3)	1.370	1.377
N(3)—C(10)	1.414(3)	1.411	1.411	1.408(2)	1.409	1.409	1.405(3)	1.405	1.406
N(3)—C(4)	1.354(3)	1.370	1.375	1.365(2)	1.374	1.378	1.369(2)	1.381	1.384
N(3)—C(12)	1.456(3)	1.456	1.452	1.454(2)	1.450	1.451	1.445(3)	1.449	1.449
C(4)—C(5)	1.539(3)	1.540	1.538	1.535(2)	1.541	1.539	1.537(3)	1.542	1.540
C(5)—C(11)	1.519(3)	1.520	1.520	1.511(2)	1.520	1.520	1.513(3)	1.521	1.520
C(5)—C(13)	1.541(3)	1.547	1.547	1.538(2)	1.548	1.548	1.530(3)	1.544	1.544
C(5)—C(14)	1.536(3)	1.546	1.546	1.533(3)	1.544	1.545	1.538(4)	1.548	1.548
C(6)—C(7)	1.395(3)	1.400	1.405	1.388(3)	1.400	1.405	1.386(4)	1.401	1.405
C(6)—C(11)	1.376(3)	1.382	1.389	1.376(2)	1.384	1.389	1.381(3)	1.384	1.388
C(7)—C(8)	1.392(3)	1.399	1.398	1.374(3)	1.392	1.398	1.366(4)	1.392	1.398
C(8)—C(9)	1.393(3)	1.398	1.402	1.387(3)	1.398	1.402	1.386(4)	1.399	1.403
C(9)—C(10)	1.390(3)	1.390	1.395	1.380(2)	1.390	1.395	1.386(3)	1.391	1.396
C(10)—C(11)	1.382(3)	1.394	1.401	1.382(2)	1.395	1.401	1.379(3)	1.396	1.402
C(15)—C(20)	1.398(3)	1.400	1.405	1.388(2)	1.401	1.407	1.399(3)	1.406	1.411
C(16)—C(15)	1.394(3)	1.396	1.402	1.386(2)	1.401	1.407	1.382(3)	1.397	1.403
C(16)—C(17)	1.385(3)	1.391	1.395	1.376(3)	1.390	1.394	1.389(3)	1.394	1.398
C(17)—C(18)	1.384(3)	1.386	1.391	1.366(3)	1.390	1.395	1.378(3)	1.397	1.404
C(18)—C(19)	1.381(3)	1.388	1.393	1.372(3)	1.392	1.397	1.384(3)	1.403	1.408
C(19)—C(20)	1.380(3)	1.386	1.391	1.375(3)	1.387	1.391	1.372(3)	1.381	1.385
r^{a}		0.9963	0.9958		0.9957	0.9950		0.9953	0.9942
Bond angles									
O(1)—C(1)—C(15)	117.0(1)	117.3	117.4	115.6(2)	116.6	116.7	118.3(2)	118.2	118.2
O(1)—C(1)—C(2)	126.5(2)	125.9	125.9	127.0(2)	126.4	126.4	125.3(2)	124.6	124.6
C(1)—C(2)—C(4)	128.9(2)	128.4	128.4	127.7(2)	128.2	128.2	129.4(2)	128.5	128.4
C(1)—C(15)—C(20)	118.5(1)	117.3	117.0	116.7(2)	116.8	116.5	118.6(2)	117.6	117.3
C(1)—C(15)—C(16)	122.8(1)	123.8	124.1	124.3(2)	124.5	124.8	123.9(2)	124.6	124.8
C(2)—C(4)—N(3)	121.7(1)	121.1	121.0	122.3(2)	121.0	120.9	121.1(2)	121.2	121.1
C(2)—C(4)—C(5)	130.3(1)	130.8	130.8	129.3(2)	130.8	130.9	130.9(2)	130.9	131.0
C(2)—C(1)—C(15)	116.4(1)	116.8	116.7	117.4(2)	117.0	116.7	116.4(2)	117.2	117.2
N(3)—C(10)—C(11)	108.7(1)	108.8	108.7	108.9(2)	108.8	108.6	108.9(2)	108.9	108.8
N(3)—C(4)—C(5)	107.9(1)	108.1	108.1	108.3(2)	108.3	108.3	107.9(2)	107.9	107.9
N(3)C(10)—C(9)	128.9(2)	129.2	129.3	128.8(2)	129.2	129.2	128.6(2)	129.3	129.4
C(4)—N(3)—C(10)	111.8(1)	111.9	111.9	111.9(2)	111.9	111.9	111.8(2)	111.9	111.9
C(4)—C(5)—C(11)	101.6(1)	101.5	101.7	101.4(2)	101.5	101.7	101.4(2)	101.6	101.8
C(4)—C(5)—C(13)	111.7(1)	111.1	111.0	111.3(2)	111.2	111.2	111.4(2)	112.0	111.8
C(4)—C(5)—C(14)	111.2(1)	111.9	111.7	112.1(2)	111.7	111.5	111.0(2)	111.1	111.0
C(4)—N(3)—C(12)	124.8(1)	124.1	123.9	124.8(2)	124.0	124.0	124.1(2)	124.0	123.8
C(5)—C(11)—C(6)	130.4(2)	130.5	130.6	130.2(2)	130.5	130.6	130.9(2)	130.5	130.5
C(5)—C(11)—C(10)	109.8(1)	109.6	109.6	109.5(2)	109.6	109.6	110.0(2)	109.6	109.6
C(6)—C(7)—C(8)	120.6(2)	120.2	120.3	119.8(2)	120.3	120.4	120.3(2)	120.2	120.2
C(6)—C(11)—C(10)	119.7(2)	120.0	119.9	120.3(2)	119.9	119.8	119.2(2)	119.9	119.9
C(7)—C(8)—C(9)	121.4(2)	121.1	121.2	121.7(2)	121.1	121.1	121.8(2)	121.1	121.2
C(7)—C(6)—C(11)	118.8(2)	119.2	119.1	119.1(2)	119.2	119.1	119.4(2)	119.3	119.2
C(8)—C(9)—C(10)	117.0(2)	117.6	117.5	116.8(2)	117.6	117.4	116.8(2)	117.7	117.6
C(9)—C(10)—C(11)	122.4(2)	121.9	122.0	122.3(2)	122.0	122.1	122.5(2)	121.8	121.9
C(10)—N(3)—C(12)	123.3(1)	124.0	124.2	123.3(2)	124.1	124.1	124.0(2)	124.2	124.3
C(11)—C(5)—C(13)	110.0(1)	110.1	110.1	109.7(2)	110.7	110.4	110.7(2)	110.9	111.0
C(11)—C(5)—C(14)	110.1(1)	111.9	112.0	110.1(2)	110.3	110.7	109.8(2)	110.0	110.0
C(13)—C(5)—C(14)	111.8(1)	111.1	111.0	111.7(2)	111.1	111.0	112.1(2)	111.0	110.9
C(15)—C(16)—C(17)	120.7(2)	120.9	120.9	119.1(2)	119.7	119.7	121.7(2)	121.6	121.6
C(15)—C(20)—C(19)	120.9(2)	121.0	121.0	119.5(2)	119.8	119.8	121.3(2)	121.4	121.4
C(16)—C(17)—C(18)	118.8(2)	118.7	118.7	123.2(2)	122.6	122.7	119.4(2)	119.6	119.6
C(16)—C(15)—C(20)	118.7(2)	118.9	118.9	119.0(2)	118.7	118.7	117.5(2)	117.8	117.8
C(17)—C(18)—C(19)	122.2(2)	121.3	122.0	116.2(2)	116.6	116.6	119.9(2)	119.5	119.6
C(18)—C(19)—C(20)	118.5(2)	118.6	118.9	123.0(2)	122.6	122.7	120.1(2)	120.1	120.5
r^{a}		0.9963	0.9960		0.9965	0.9961		0.9973	0.9969
Torsion angles									
O(1)—C(1)—C(2)—C(4)	−6.3(3)	−5.96	−4.9	5.8(4)	−3.2	−2.2	4.6(4)	7.4	6.3
O(1)—C(1)—C(15)—C(20)	−32.1(2)	−21.2	−19.4	−16.4(3)	−14.6	−11.7	24.8(3)	16.0	14.2
C(1)—C(2)—C(4)—C(5)	−3.5(3)	−3.1	−2.4	−0.7(4)	−0.8	−0.2	3.0(4)	3.0	2.4
O(2)—N(1)—C(18)—C(17)	−7(1)	0.1	0.4						
O(2)—N(1)—C(18)—C(17)				−13.6(3)	0.1	−0.4			
O(4)—N(2)—C(19)—C(18)				−15.8(3)	−0.3	−0.1			
C(21)—O(2)—C(18)—C(17)							2.9(3)	−0.4	−0.3

[a] Correlation coefficient.

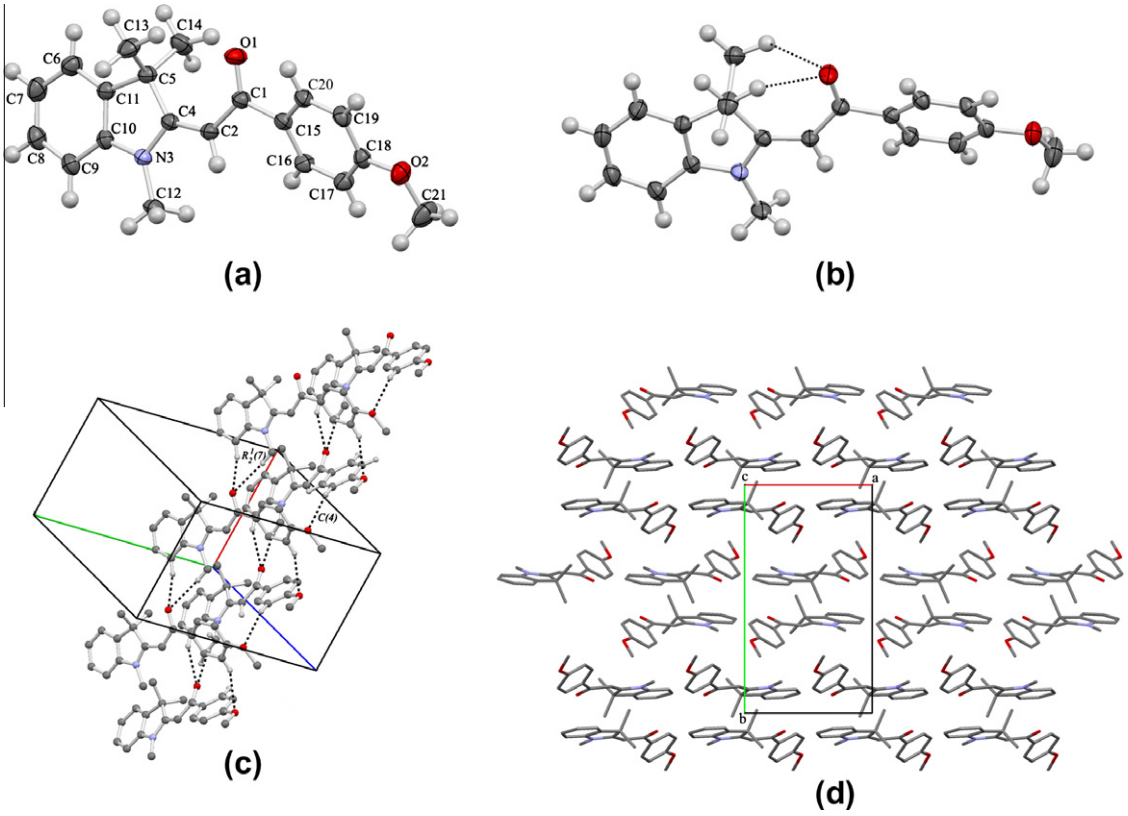

Fig. 5. (a) Molecular structure of **3c** at 30% of probability level and atom numbering. (b) Intramolecular hydrogen bonds, view along C(13)—C(5) bond. (c) Visualization of C—H···O interactions as well as the intermolecular ring and chain formed. (d) Packing patter view along *a* axis, hydrogen atoms were omitted for clarity.

Table 4
Dimensions of short contacts of the crystal structures and the optimized geometries with B3LYP/6-311G(d,p) and PW91/6-311G(d,p) of **1c**, **2c** and **3c** compounds.

Crystal		D–H···A (*symmetry codes*)	D–H (Å)	H···A (Å)	D···A (Å)	DH···A (°)
1c	X-ray	C13—H13C···O1[a]	0.960(2)	2.333(1)	3.099(2)	136.3(1)
		C14—H14B···O1[a]	0.960(2)	2.367(1)	3.125(2)	136.5(1)
		C20—H20···O2 (−*x*, 1 − *y*, 1 − *z*)	0.930(2)	2.579(1)	3.343(2)	139.7(1)
		C16—H16···O2B (1 − *x*, 1 − *y*, 2 − *z*)	0.930(2)	2.69(1)	3.39(1)	132.6(4)
	B3LYP[a]	C13—H13C···O1[a]	1.088	2.260	3.101	132.6
		C14—H14B···O1[a]	1.088	2.283	3.115	131.7
	PW91[a]	C13—H13C···O1[a]	1.095	2.238	3.095	133.4
		C14—H14B···O1[a]	1.095	2.268	3.114	132.4
2c	X-ray	C13—H13C···O1[a]	0.980(2)	2.278(1)	3.052(3)	135.2(1)
		C14—H13B···O1[a]	0.980(2)	2.278(1)	3.053(2)	135.2(1)
		C12—H12A···O3 (−*x*, −*y*, 1 − *z*)	0.979(2)	2.565(1)	3.437(2)	148.3(1)
		C7—H7···O3 (*x*, *y*,−1 + *z*)	0.949(2)	2.513(2)	3.417(3)	159.2(1)
		C8—H8···O4 (*x*, −1 + *y*, −1 + *z*)	0.949(2)	2.691(2)	3.373(3)	129.3(8)
	B3LYP	C13—H13C···O1[a]	1.088	2.258	3.097	132.4
		C14—H14B···O1[a]	1.088	2.280	3.111	131.6
	PW91	C13—H13C···O1[a]	1.095	2.241	3.095	133.2
		C14—H14B···O1[a]	1.095	2.265	3.111	132.4
3c	X-ray	C13—H13A···O1[a]	1.03(3)	2.36(3)	3.100(3)	133(2)
		C13—H13A···O2[a]	1.03(3)	2.32(3)	3.156(3)	131(2)
		C9—H9···O1 (−1 + *x*, *y*, *z*)	0.99(3)	2.62(3)	3.533(3)	153(2)
		C12—H12A···O1 (−1 + *x*, *y*, *z*)	0.95(3)	2.65(3)	3.572(3)	165(2)
		C17—H17···O2 (−1/2 + *x*, 1/2 + *y*, *z*)	0.93(2)	2.68(3)	3.532(3)	153(2)
	B3LYP[a]	C13—H13C···O1[a]	1.088	2.274	3.104	131.6
		C14—H14B···O1[a]	1.088	2.250	3.091	132.5
	PW91[a]	C13—H13C···O1[a]	1.095	2.255	3.101	132.4
		C14—H14B···O1[a]	1.096	2.230	3.086	133.3

[a] Intramolecular.

For compound **3c**, the supramolecular arrangement shows that the C(9) and C(12A) atoms at (x, y, z) act as a contact donor with the same carbonyl O(2) atom in the molecule at ($-1+x$, y, z), and these interactions lead to the formation of ring $R_2^1(7)$ (Fig. 5c; Table 4). In addition, the methoxy O(1) atom at (x, y, z) acts as an acceptor of the donor C(11) atom at ($1/2+x$, $1/2-y$, z), and by translation a chain *C*(*4*) is formed. Both motifs are running parallel to *a* axis.

3.3. Experimental FTIR results

The FTIR data of compounds **1c**, **2c** and **3c** are listed in Table 5 and the spectra showed in Figs. 6*i*, *iv* and *vii*, respectively. The main signals are grouped in two regions, in the range of 3200–2800 cm^{-1} and from 1700 cm^{-1} to 550 cm^{-1}. The second region shows vibrational bands strongly mixed, therefore, the assignment of the experimental bands was made by comparison with a visualization of the shape of the different molecular vibrational modes theoretically calculated for each structure.

Region 3200–2800 cm^{-1}. The weak bands observed from 3150 to 3000 cm^{-1}, can be assigned to the aromatic C—H bonds in-plane stretching modes, as well as those corresponding to C—H stretching vibrational modes of the exocyclic alkene of the indoline moiety. From 3000 to 2800 cm^{-1}, the corresponding symmetric and asymmetric C—H stretching bands of the methyl groups are observed. These weak bands resemble the frequencies recently reported in the literature for 2,2′-(1,4-phenylenedivinylene)bis-1,3,3-trimethyl-indolenine dichloride [3].

Region 1700–550 cm^{-1}. The bands observed here show a conjugated carbonyl weak stretching band between 1625 and 1615 cm^{-1}. Aromatic C=C stretching weak bands are observed in the range of 1598 to 1542 cm^{-1}. The corresponding very strong bands for aliphatic C=C bonds are located from 1527 to 1516 cm^{-1} [28]. The band corresponding to the N=O asymmetric stretching was not observed due to potential overlapping by C=C phenyl stretching bands appearing on the same region.

Medium bands corresponding to asymmetric and symmetric C—H bending modes of methyl groups can be observed in the interval of 1500 and 1300 cm^{-1}. The N=O symmetric stretching band is strong and observed around 1340 cm^{-1} in both **1c** and **2c**. Aromatic C—H in-plane bending vibrations are typical of this spectral region.

From to 1300 to 1000 cm^{-1}, the bands corresponding to symmetric and asymmetric C—O—C vibrations of the methoxy group attached to the aromatic ring in **3c** are observed. The symmetric stretching vibration appears in 1248 cm^{-1} and the asymmetric one in 1032 cm^{-1}.

The region below 1000 cm^{-1}, exhibits the out of plane bending C—H bond vibrations of the aromatic and alkene carbon double bonds.

3.4. Geometrical analysis

The calculated structural parameters of **1c**, **2c** and **3c** are listed in Table 3. These results clearly resemble those obtained by the crystal structure data analysis, a clear evidence of the proper choice of the applied model. From these data one can clearly realize that in general the calculated bond distances and angles are slightly larger than those determined by single crystal X-ray diffraction techniques. This being mainly due to the fact that theoretical calculations model isolated molecules in the gas phase, rather than molecules in a close packing environment.

The largest differences between the experimental and calculated bond lengths are for **1c** with B3LYP and PW91, 0.018 Å and 0.021 Å, for **2c**, 0.024 Å and 0.029 Å, and for **3c**, 0.026 Å y 0.032 Å, respectively (Table 3). In addition, the largest angle value differences are for **1c** with B3LYP and PW91, 1.80° and 1.81°, for **2c**, 1.40° and 1.55° and for **3c**, 1.20° and 1.26°, respectively. The correlation coefficients r between the experimental and the different calculated geometric parameters were processed for the two functionals [33] (Table 3). The data reflect that the two methods correlate well for the bond lengths and angles, being the B3LYP functional approach the best, indicating the calculation precision to be satisfactory.

Selected dihedral angles (Table 3), presented a pronounced difference between experimental and calculated results. In compound **1c**, the largest deviation of the torsion angle O(1)—C(1)—C(15)—C(20) with B3LYP and PW91 is of 10.91° and 12.73°, respectively. In the same manner, the nitro group presents a deviation of about 7° in the calculated torsion angle O(2)—N(1)—C(18)—C(17) respect to the experimental data. For compound **2c**, the main difference between calculated and experimental data is denoted by the inverted sense of rotation of the torsion angles O(1)—C(1)—C(2)—C(4), which showed a deviation of 9° and 8°, with B3LYP and PW91, respectively (Table 3). In spite of this, the angle torsion O(1)—C(1)—C(15)—C(20) is only slightly different from the experimental. The two nitro groups do not show a different trend of the planarity deviation commented above, in fact, the difference is larger in the torsion angle O(2)—N(1)—C(18)—C(17) being roughly 13°, and 15° for the O(4)—N(2)—C(19)—C(18) dihedral angle. For **3c**, the largest difference in torsion is present around the C(1)—C(15) bond compare 8.78° and 10.64° in the torsion angle O(1)—C(1)—C(15)—C(20) for B3LYP and PW91, respectively. However, the change in the torsion angle C(21)—O(2)—C(18)—C(17) of the methoxy group is of only 3.2°, but in different sense of rotation.

3.5. Vibrational and structural analysis

The calculated frequencies for the three compounds are listed in Table 5, these results reveal a substantial difference in comparison with the experimental values, due to neglection of harmonicity in real systems. The calculated frequencies using the B3LYP functional present an overestimation slightly larger than the values calculated with the PW91 functional.

The overestimation of the computed wavenumbers is systematic and can be corrected by applying appropriate scaling factors or scaling equations [34]. The values of the wavenumbers scaled by two factors (ν_{scal}) for the data calculated with the B3LYP/6-311G(d,p) and PW91/6-311G(d,p) methods are listed in Table 5. Scott and Radom recommended scaling factors for HF and DFT calculated frequencies [35]. However, there is no scaling factor for B3LYP/6-311G(d,p) and PW91/6-311G(d,p), so the corresponding to B3LYP/6-31G(d) and B3PW91/6-31G(d) factors were used, 0.9614 and 0.9573, respectively. The scaling equation procedure suggested by Alcolea Palafox was used to obtain the predicted frequencies [36,37] and they are listed in Table 5 as ν_{scaleq}. The equations used were, for B3LYP/6-311G(d,p) $\nu_{scaleq} = 17.8 + 0.9614\nu_{calc}$ and for PW91/6-311G(d,p) $\nu_{scaleq} = 24.8 + 0.9501\nu_{calc}$. Both functionals and both scaling procedures, reproduce wavenumbers with comparable r.m.s. errors also listed in Table 5, and both can be used for theoretical prediction of the FTIR spectra. The FTIR vibrational frequency for the carbonyl bond C1—O1 for the three structures presents a maximum difference of 72 and 15 cm^{-1} when the B3LYP/6-311G(d,p) and PW91/6-311G(d,p) levels are applied.

The experimental absorption frequencies, corresponding to the non-planar conjugated systems, show that the carbonyl, aromatic and aliphatic carbon–carbon double bond stretching bands appear in the region from 1630 cm^{-1} to 1500 cm^{-1} for the three compounds (Fig. 6; Table 5). This region corresponds to the group of frequencies that allow observing conformational transitions for α,β-unsaturated compounds.

Taking into account that the phenyl group of the ketone decreases the planar conformation of the three structures due to

Table 5
Observed and calculated B3LYP/6-311G(d,p) and PW91/6-311G(d,p) vibrational frequencies (cm^{-1}) for **1c**, **2c** and **3c**.

Exp	B3LYP			PW91			Exp	B3LYP			PW91			Exp	B3LYP			PW91			Assignments
FTIR	ν_{calc}	ν_{scal}[a]	ν_{scaleq}[b]	ν_{calc}	ν_{scal}[c]	ν_{scaleq}[d]	FTIR	ν_{calc}	ν_{scal}[a]	ν_{scaleq}[b]	ν_{calc}	ν_{scal}[c]	ν_{scaleq}[d]	FTIR	ν_{calc}	ν_{scal}[a]	ν_{scaleq}[b]	ν_{calc}	ν_{scal}[c]	ν_{scaleq}[d]	
1c							***2c***							***3c***							
3086, vw	3207	3083	3101	3133	2999	3001	3110, vw	3236	3111	3129	3158	3023	3025	3056, vw	3207	3083	3101	3136	3002	3004	νC—H ip of C=C
3042, vw	3187	3064	3082	3129	2995	2998	3082, w	3191	3068	3086	3140	3006	3008	3042, vw	3203	3079	3097	3129	2995	2998	νC—H ip of phenyls
3007, vw	3166	3044	3062	3097	2965	2967	3008, vw	3168	3046	3064	3110	2977	2980	3005, w	3135	3014	3032	3106	2973	2976	νC—H ip aromatic rings
2964, vw	3097	2977	2995	3053	2923	2925	2960, w	3160	3038	3056	3051	2921	2924	2960, w	3149	3027	3045	3092	2960	2963	ν_{as}C—H of CH_3
2922, vw	3076	2957	2975	3021	2892	2895	2925, vw	3080	2961	2979	3025	2896	2899	2929, vw	3134	3013	3031	3002	2874	2877	ν_{as}C—H of CH_3
								3039	2922	2939	2983	2856	2859	2919, w	3036	2919	2937	3002	2874	2877	ν_sC—H of CH_3
2884, vw	3035	2918	2936	2983	2856	2859	2865, vw	3036	2919	2937	2981	2854	2857	2884, vw	3015	2899	2916	2980	2853	2856	ν_sC—H of CH_3
2855, vw	3023	2906	2924	2965	2838	2842								2832, vw	3002	2886	2904	2941	2815	2819	ν_sC—H of CH_3
1625, w	1687	1622	1640	1625	1556	1569	1615, m	1687	1622	1640	1628	1558	1572	1622, w	1684	1619	1637	1624	1555	1568	νC=O
1594, w	1648	1584	1602	1603	1535	1548	1581, m	1654	1590	1608	1614	1545	1558	1598, m	1646	1582	1600	1603	1535	1548	νC=C ip aromatic rings
	1643	1580	1597	1593	1525	1538		1636	1573	1591	1581	1513	1527								νC=C ip phenyl rings + ν_{as}N=O
														1573, m	1604	1542	1560	1564	1497	1511	νC=C ip aromatic rings
							1542, sh	1609	1547	1565	1546	1480	1494								νC=C ip phenyl rings + ν_{as}N=O
1518, vs	1578	1517	1535	1553	1487	1500	1516, vs	1579	1518	1536	1555	1489	1502	1527, vs	1583	1522	1540	1551	1485	1498	νC=C
				1533	1468	1481															ν_{as}N=O
														1504, m	1539	1480	1497	1491	1427	1441	δC—H ip phenyl ring
1488, m	1523	1464	1482	1480	1417	1431	1485, m	1525	1466	1484	1478	1415	1429	1493, m	1524	1465	1483	1476	1413	1427	δ_{as}C—H of CH_3
1457, m	1490	1432	1450	1451	1389	1403	1450, m	1492	1434	1452	1452	1390	1404	1452, m	1491	1433	1451	1451	1389	1403	Indole skeletal vibration
1435, w	1466	1409	1427	1416	1356	1370	1419, w	1478	1421	1439	1440	1379	1393	1437, w	1465	1408	1426	1416	1356	1370	δ_sC—H of CH_3
							1378, m	1387	1333	1351	1352	1294	1309	1405, w	1433	1378	1395	1394	1334	1349	νC=C ip phenyl rings
1369, m	1410	1356	1373	1349	1291	1306								1365, s	1392	1338	1356	1356	1298	1313	δ_sC—H of CH_3
														1351, s	1375	1322	1340	1340	1283	1298	δC—H ip indole ring
1343, s	1377	1324	1342	1311	1255	1270	1337, s	1386	1333	1350	1319	1263	1278								ν_sN=O
								1375	1322	1340	1311	1255	1270								ν_sN=O
1317, m	1326	1275	1293	1301	1245	1261	1293, m	1326	1275	1293	1299	1244	1259								Skeletal vibration
														1310, w	1348	1296	1314	1348	1290	1306	νC=C ip phenyl ring
1297, w	1297	1247	1265	1261	1207	1223	1275, m	1299	1249	1267	1260	1206	1222	1299, w	1330	1279	1296	1304	1248	1264	δC—H ip aromatic rings
1275, w	1264	1215	1233	1226	1174	1190	1248, w	1263	1214	1232	1226	1174	1190								δ_sC—H of $C(CH_3)_2$
														1248, s	1281	1232	1249	1250	1197	1212	$\nu_{as}C_{ar}$—O—C_{al}
1207, s	1219	1172	1190	1188	1137	1154								1215, s	1230	1183	1200	1202	1151	1167	Phenyl skeletal vibration
							1233, w	1251	1203	1221	1200	1149	1165								δC—H ip phenyl ring
1187, w	1207	1160	1178	1173	1123	1139								1188, vs	1262	1213	1231	1226	1174	1190	δ_sC—H of $C(CH_3)_2$
							1218, m	1230	1183	1200	1189	1138	1154								δC—H ip phenyl ring
							1183, w	1207	1160	1178	1172	1122	1138	1174, vs	1207	1160	1178	1172	1122	1138	δ_sC—H of $C(CH_3)_2$
1176, w	1198	1152	1170	1159	1110	1126								1154, w	1195	1149	1167	1156	1107	1123	δC—H ip phenyl ring
1160, w	1186	1140	1158	1153	1104	1120	1161, w	1185	1139	1157	1155	1106	1122								δC—H ip indole ring
1132, m	1153	1108	1126	1121	1073	1090	1132, m	1152	1108	1125	1122	1074	1091	1134, m	1153	1108	1126	1121	1073	1090	Skeletal vibration of indole
							1118, w	1143	1099	1117	1108	1061	1078								Skeletal vibration
1106, w	1127	1083	1101	1083	1037	1054															Skeletal vibration
							1088, w	1110	1067	1085	1070	1024	1041	1117, m	1144	1100	1118	1098	1051	1068	δC—H ip phenyl ring
1068, m	1085	1043	1061	1056	1011	1028	1071, m	1082	1040	1058	1061	1016	1033								δC—H ip phenyl ring
	1068	1027	1045	1042	998	1015		1068	1027	1045	1044	999	1017		1068	1027	1045	1034	990	1007	νC—N of phenyl ring and def
	1047	1007	1024											1107, m	1132	1088	1106	1074	1028	1045	Skeletal vibration
1049, w	1031	991	1009	1024	980	998	1048, w	1046	1006	1023	1023	979	997	1050, w	1068	1027	1045	1043	998	1016	Deformation vibration indole
							1021, w	1016	977	995	988	946	963								Phenyl deformation vibration
														1032, s	1058	1017	1035	1031	987	1004	ν_sC_{ar}—O—C_{al}
							974, vw	982	944	962	944	904	922								δC—H oop indole ring
1010, w	1010	971	989	971	930	947								978,w	997	959	976	959	918	936	δC—H oop phenyl ring
							941, m	956	919	937	928	888	906								Skeletal vibration
							917, m	929	893	911	896	858	876	929, m	940	904	922	920	881	899	Phenyl def vibration
933, m	942	906	923	933	893	911															Indole skeletal vibration
							903, m	861	828	846	833	797	816	855, vs	901	866	884	877	840	858	Skeletal vibration

							837, m	815	784	801	785	751	771	848, vs	868	834	852	836	800	819	δC—H oop=CH and ar CH
886, m	903	868	886	881	843	862	793, m	778	748	766	776	743	762	797, vs	823	791	809	792	758	777	Skeletal vibration
868, m	894	859	877	860	823	842															δC—H oop phenyl ring
848, s	867	834	851	840	804	823															Skeletal vibration
804, m	825	793	811	793	759	778															δC—H oop=CH and ar CH
							781, m	765	735	753	737	706	725								δC—H oop=CH and ar CH
744, s	754	725	743	726	695	715	751, m	755	726	744	727	696	716	744, vs	751	722	740	725	694	714	δC—H oop indol phenyl ring
718, m	726	698	716	700	670	690	742, s	739	710	728	718	687	707	703, m	713	685	703	696	666	686	Indole skeletal vibration
							717, vs	705	678	696	685	656	676								Skeletal vibration
697, m	708	681	698	688	659	678	684, m	608	585	602	591	566	586								Skeletal vibration
														679, m	702	675	693	678	649	669	δC—H oop=CH and ar CH
685, w	682	656	673	670	641	661	649, w	488	469	487	472	452	473	637, m	685	659	676	661	633	653	Skeletal vibration
	70.8	29.4	25.7	44.6	62.0	48.5		74.3	47.0	41.3	53.3	72.7	58.5		78.7	28.0	30.5	46.3	54.1	41.6	R.m.s. error

Legends of bond types is as follows: *ν*, stretching; *δ*, bending; ip, in-plane; oop, out of plane; s, symmetrical; as, asymmetrical; def, deformation.
s, strong; vs very strong; m, medium; w, weak; vw, very weak; sh, shoulder; blank, not observed o measured.

[a] Scaling factor: 0.9614.

[b] Scaling equation: $\nu_{scaleq} = 17.8 + 0.9614\nu_{calc}$.

[c] Scaling factor: 0.9573.

[d] Scaling equation: $\nu_{scaleq} = 24.8 + 0.9501\nu_{calc}$.

Fig. 6. Experimental FTIR spectra of (*i*) **1c**, (*iv*) **2c**, and (*vii*) **3c**. Calculated spectrum by the B3LYP/6-311G(d,p) method of (*ii*) **1c**, (*v*) **2c**, and (*viii*) **3c**. Calculated spectrum of by the PW91/6-311G(d,p) method of (*iii*) **1c**, (*vi*) **2c**, and (*ix*) **3c**.

ability to rotate of the single bond C(1)—C(15), the possibility of free rotation around C(2)—C(1) bond is sterically hindered because of the bulky aromatic ring (Fig. 2b and d). In addition, the α,β-unsaturated non-planar structures of **1c**, **2c**, ad **3c** diminish the conjugation effect [38,39]; therefore, the probability of having both conformations *s-cis* and *s-trans* is low, being this the reason of the presence of only one vibration band assigned to the carbonyl stretching in the *s-cis* conformation. This being in agreement with the fact that for α,β-unsaturated compounds, the vibrational band for the C= C bond conjugated with a C=O bond in a *s-cis* conformation has the particularity of appearing as a very strong band below 1600 cm^{-1} or downshifted near to 1500 cm^{-1} if conjugation in the system is increased [12]. Hence, the presence of a strong band in the three FTIR spectra reveals that the unique molecular conformation in the solid state is *s-cis* with *E* configuration.

Table 6
Experimental (δ_{exp}) and predicted (δ_{pred}) ^{1}H and ^{13}C chemical shifts (ppm), and calculated GIAO isotropic magnetic shielding tensors (σ_{calc}) for compounds **1c**, **2c** and **3c**.

Parameter	B3LYP			PW91		B3LYP			PW91		B3LYP			PW91	
	δ_{exp}[e]	δ_{pred}[f]	σ_{calc}	δ_{pred}[f]	σ_{calc}	δ_{exp}[e]	δ_{pred}[f]	σ_{calc}	δ_{pred}[f]	σ_{calc}	δ_{exp}[e]	δ_{pred}[f]	σ_{calc}	δ_{pred}[f]	σ_{calc}
Proton	***1c***					***2c***					***3c***				
C(2)—H	5.91	6.02	25.3082	6.35	24.5743	5.92	6.04	25.2056	6.40	24.4568	5.94	6.10	25.2890	6.39	24.6061
C(6)—H	7.24	7.15	24.0983	7.10	23.7931	7.27	7.04	24.0950	7.02	23.7785	7.18	7.18	24.1605	7.11	23.8616
C(7)—H	7.06	6.96	24.3042	6.91	23.9868	7.12	6.92	24.2271	6.90	23.9173	6.99	6.93	24.4143	6.88	24.0973
C(8)—H	7.25	7.12	24.1341	7.05	23.8447	7.31	7.05	24.0825	7.00	23.8009	7.19	7.14	24.1974	7.07	23.9099
C(9)—H	6.85	6.63	24.6618	6.57	24.3449	6.92	6.62	24.5634	6.59	24.2492	6.77	6.60	24.7601	6.54	24.4517
C(12)—H	3.34	3.17	28.3555	3.14	27.9500	3.42	3.30	28.2429	3.27	27.8322	3.29	3.12	28.3986	3.10	28.0040
C(13)—H	1.85	2.04	29.5630	2.01	29.1400	1.86	2.08	29.5883	2.04	29.1641	1.78	1.82	29.7590	1.82	29.3176
C(14)—H	1.85	1.91	29.7067	1.91	29.2500	1.86	2.01	29.6613	2.00	29.2129	1.78	2.01	29.5543	2.01	29.1242
C(16)—H	8.04	7.76	23.4489	7.76	23.0993	9.06	9.01	21.9193	8.97	21.6768	7.94	7.86	23.4469	7.86	23.0903
C(17)—H	8.24	8.38	22.7846	8.33	22.4915						6.91	6.58	24.7875	6.60	24.3939
C(18)—H						9.10	9.29	21.6087	9.21	21.4166					
C(19)—H	8.24	8.46	22.7047	8.41	22.4073						6.91	6.99	24.3593	6.94	24.0359
C(20)—H	8.04	8.31	22.8576	8.34	22.4868	9.06	9.50	21.3767	9.50	21.0993	7.94	8.35	22.9307	8.35	22.5861
C(21)—H											3.82	3.77	27.7157	3.78	27.3011
a[a]			29.688		29.717			28.810		29.024			30.295		30.259
b[b]			−0.9351		−0.9507			−0.9034		−0.9252			−0.9569		−0.9700
r[c]			−0.9970		−0.9951			−0.9961		−0.9944			−0.9963		−0.9946
R.m.s.[d]		0.19		0.24			0.24		0.29			0.20		0.21	
Carbon-13															
C(1)	184.2	180.2	−5.9976	179.8	−2.4581	180.1	175.3	−1.3824	174.6	2.3822	185.6	180.4	−6.8491	179.7	−2.9073
C(2)	90.4	91.1	86.8959	93.2	84.9245	88.7	87.2	90.8200	90.1	88.0392	90.4	91.1	86.9337	92.2	85.9457
C(4)	174.1	175.1	−0.6604	172.8	4.5958	175.5	176.3	−2.4083	174.2	2.7775	171.7	171.9	2.0765	169.8	7.1132
C(5)	48.7	53.9	125.6995	54.4	124.0462	49.1	53.9	125.6913	54.6	124.0378	48.5	53.1	126.7906	53.7	125.0925
C(6)	123.0	122.7	53.9595	122.4	55.4896	123.5	122.2	54.2088	121.7	55.9452	121.9	122.4	54.1069	122.1	55.5946
C(7)	121.9	121.9	54.7782	122.5	55.3649	119.7	122.5	53.8441	122.7	54.9210	114.0	120.5	56.0680	121.1	56.5565
C(8)	127.5	127.6	48.8549	127.6	50.2387	127.6	127.8	48.3566	127.4	50.1741	127.3	127.0	49.2348	127.0	50.5736
C(9)	108.0	106.2	71.1312	106.1	71.8593	108.4	107.1	69.9601	106.7	71.1625	107.4	105.3	72.0308	105.2	72.7832
C(10)	147.7	143.8	31.9038	143.9	33.7180	145.6	143.2	32.2080	143.3	34.0647	143.6	143.8	31.5489	143.8	33.5711
C(11)	140.1	142.3	33.4965	143.5	34.1742	140.0	142.3	33.0995	143.5	33.8203	139.8	142.0	33.4358	143.1	34.1921
C(12)	29.8	27.8	152.9089	27.5	1511830	30.7	28.4	152.3410	28.5	150.4767	29.7	28.3	152.8858	27.7	151.4521
C(13)	22.7	23.1	157.7915	22.2	156.6184	22.5	22.5	158.5203	21.4	157.6267	23.6	21.2	160.3591	20.2	159.0486
C(14)	22.7	20.3	160.7118	19.5	159.3081	22.5	21.0	160.1160	20.5	158.5761	23.6	24.7	156.6607	23.9	155.3361
C(15)	142.9	148.0	27.5437	146.8	30.7709	142.6	143.6	31.7578	144.4	32.9681	132.6	135.1	40.7370	135.5	41.9427
C(16)	128.1	124.2	52.3679	124.2	53.5829	127.4	126.8	49.3897	125.6	52.0076	129.3	126.8	49.4251	126.1	51.5528
C(17)	123.3	123.1	53.5303	123.2	54.6728	148.3	148.0	27.2185	149.8	27.4879	113.1	105.2	72.1591	105.4	72.5135
C(18)	148.7	149.9	25.6074	151.0	26.5576	121.9	120.9	55.5650	119.2	58.4611	162.1	162.1	12.3591	163.2	13.7660
C(19)	123.3	124.6	51.9507	124.9	52.9370	148.3	149.8	25.2613	151.9	25.3863	113.1	116.5	60.3039	117.1	60.6610
C(20)	128.1	129.7	46.6777	129.8	47.9444	127.4	131.2	44.7499	129.6	47.9522	129.3	131.2	44.8659	130.5	47.0740
C(21)											55.6	53.7	126.2352	55.0	123.7528
a			174.42		177.33			173.98		176.90			173.89		176.80
b			−0.9591		−0.9908			−0.9557		−0.9862			−0.9524		−0.9844
r			−0.9985		−0.9982			−0.9988		−0.9983			−0.9977		−0.9972
R.m.s.		2.63		2.88			2.34		2.80			3.28		3.61	

[a] Slope.
[b] Intercept.
[c] Correlation coefficient.
[d] Root mean square error.
[e] Experimental.
[f] Scaling equation: $\delta_{pred} = a + b\sigma_{calc}$.

3.6. ^{1}H and ^{13}C NMR analysis

The relations between the experimental ^{1}H and ^{13}C chemical shifts (δ_{exp}) and the (GIAO Gauge-Independent Atomic Orbital) magnetic isotropic shielding tensors (σ_{calc}), which are now widely used in efficient implementation [40,41], are usually linear and described by the following equation: $\delta_{exp} = a + b\sigma_{calc}$. The slope and intercept of the least-square correlation line is used to scale the GIAO isotropic absolute shielding, σ, and to predict chemical shifts, $\delta_{pred} = a + b\sigma_{calc}$ (Fig. S1 of the Supplementary information). In the present case, for the three compounds **1c**, **2c** and **3c**, the r.m.s. error denotes a very small difference when comparing calculated *versus* experimental data, finding that the better calculations are obtained with the B3LYP functional, for both ^{13}C and ^{1}H (Table 6). The same behavior is showed by the correlation coefficients *r*, denoting that the B3LYP/6-311++G(3df,3pd) and PW91/6-311++G(3df,3pd) methods were suitably applied and reproduce well the experimental chemical shifts for both nuclei.

4. Conclusions

The molecular structure of the 2,3-dihydro-2-(R-phenylacylidene)-1,3,3-trimethyl-1*H*-indole (**1c**, R = 4-NO_2; **2c**, R = 3,5-$(NO_2)_2$; **3c**, R = 4-OCH_3) derivatives have been analyzed by X-ray diffraction. The crystal structures of the three molecules showed the indole enaminoketones to be nearly planar and that the conjugative interactions lead to lengthening of the C(4)—C(2) and C(1)—O(1) bonds and shortening of the N(3)—C(4) bond due to push–pull effects. As a consequence, the phenyl group of the indole and the benzene ring of the ketone showed a significant interplanar angle, and thus no-short π–π stacking interactions are present by the aromatic rings in the crystalline arrangement of the three molecules. The geometries of the three molecules are influenced by crystal packing forces such as intermolecular short contacts that define the stacking patterns.

Optimized structures at DFT level of theory in vacuum, using the PW91 functional, are in worse disagreement with the experimental results affording slightly larger geometric parameters than those obtained with the B3LYP functional, thus allowing to conclude the latter functional to be more suitable for the systems analyzed here.

Harmonic frequencies were computed for the three compounds from optimized structures using the same level of theory, but the calculated wavenumbers are slightly higher than the experimental FTIR vibrational frequencies. Scaling factors and equations were applied to calculated data in order to resemble the real systems.

The values of the r. m. s. error concurs with the fact of experimental and calculated data to be better reproduced when calculated with the PW91 functional than with the B3LYP functional. Nevertheless, when both the scaling factors and equations are applied, the r.m.s. error denotes better data reproducibility for B3LYP than PW91.

The level of theory applied closely reproduces the FTIR spectra of the (*E*) *s-cis* structures, this being the most probable conformation of the molecules in the solid state, is unequivocally confirmed by single crystal X-ray diffraction techniques. Additionally, DFT calculations at both levels B3LYP/6-311G(d,p) and PW91/6-311G(d,p) showed minimal energy states to correspond to the aforementioned most stable (*E*) *s-cis* structure.

The magnetic isotropic shielding constants, σ_{calc}, were calculated by the GIAO/B3LYP/6-311++G(3df,3pd) and GIAO/PW91/6-311++G(3df,3pd) approaches and linear correlations with ^{1}H and ^{13}C chemical shifts were obtained. The results of the calculations confirm the high ability of the methodology applied to model the spectroscopic data of the indole derivatives studied in this work.

Acknowledgements

Financial support by CGIC-UC (Coordinación General de Investigación Científica de la Universidad de Colima, FRABA No. project 603/09) and CONACyT Grant Number 201625 for PhD formation are gratefully acknowledged. We would like to thank to Alejandrina Acosta for support in the running of the NMR spectra. Finally the authors would like to thank the Universidad de Guanajuato for allowing the use of the GAUSSIAN03.

Appendix A. Supplementary material

Supplementary data associated with this article can be found, in the online version, at doi:10.1016/j.molstruc.2010.12.001.

References

[1] V.I. Minkin, Chem. Rev. 104 (2004) 2751.
[2] H. Song, K. Chen, H. Tian, Dyes Pigments 67 (2005) 1.
[3] C. Jianzhong, K. Sung-Hoon, Chin. Sci. Bull. 49 (2004) 797.
[4] K.S. Rok, B.S. Ku, J.T. Shin, J.J. Koa, E. Buncel, Tetrahedron 61 (2005) 6720.
[5] A.A. Shimkin, V.Z. Shirinian, D.M. Nikalin, M.M. Krayushkin, T.S. Pivina, N.A. Troitsky, L.G. Vorontsova, Z.A. Starikova, Eur. J. Org. Chem. 2006 (2006) 2087.
[6] N. Corns, S.M. Partington, A.D. Towns, Color. Technol. 125 (2009) 249.
[7] K. Hunger, Industrial Dyes. Chemistry, Properties, Applications, WILEY-VCH, Weinheim, 2003.
[8] B.S. Lukyanov, M.B. Lukyanova, Chem. Heterocycl. Compd. 41 (2005) 281.
[9] D.L. Tarshits, S.Y. Tarasov, V.N. Buyanovc, Russ. Chem. Bull. 54 (2005) 2586.
[10] L.I. Kon'kov, N.M. Przhiyalgovskaya, N.N. Suvorov, Chem. Heterocycl. Compd. 5 (1984) 1130.
[11] M.A. Tlenkopatchev, Y.V. Korshak, N.T. Cegizova, G.N. Bondarenko, N.M. Prdjiylgovskay, Dokl. Akad. Nauk SSSR 291 (1986) 1428.
[12] V.N. Zemlyanoi, I.L. Mushkalo, M.Y. Kornilov, I.E. Boldeskul, M.L. Dekhtyar, Chem. Heterocycl. Compd. 19 (1983) 293.
[13] N.M. Prizhiyalgovskaya, L.I. Kon'kov, D.L. Tarshits, S.V. Salmina, N.T. Segizova, N.N. Suvorov, Chem. Heterocycl. Compd. 23 (1987) 751.
[14] M.A. Tlenkopatchev, Y.V. Korshak, E. Miranda, T. Ogawa, Polym. Bull. 34 (1995) 405.
[15] Bruker-AXS, SAINT Software Reference Manual, Bruker AXS Inc., Madison, WI, 1998.
[16] G.M. Sheldrick, Acta Crystallogr. A 46 (1990) 467.
[17] G.M. Sheldrick, SHELXL-97. Program for Crystal Structure Refinement, University of Göttingen, Germany, 1998.
[18] A. Spek, J. Appl. Crystallogr. 36 (2003) 7.
[19] L.J. Farrugia, J. Appl. Crystallogr. 32 (1999) 837.
[20] C.F. Macrae, P.R. Edgington, P. McCabe, E. Pidcock, G.P. Shields, R. Taylor, M. Towler, J. van de Streek, J. Appl. Crystallogr. 39 (2006) 453.
[21] M.J. Frisch, G.W. Trucks, H.B. Schlegel, G.E. Scuseria, M.A. Robb, J.R. Cheeseman, J.J.A. Montgomery, T. Vreven, K.N. Kudin, J.C. Burant, J.M. Millam, S.S. Iyengar, J. Tomasi, V. Barone, B. Mennucci, M. Cossi, G. Scalmani, N. Rega, G.A. Petersson, H. Nakatsuji, M. Hada, M. Ehara, K. Toyota, R. Fukuda, J. Hasegawa, M. Ishida, T. Nakajima, Y. Honda, O. Kitao, H. Nakai, M. Klene, X. Li, J.E. Knox, H.P. Hratchian, J.B. Cross, V. Bakken, C. Adamo, J. Jaramillo, R. Gomperts, R.E. Stratmann, O. Yazyev, A.J. Austin, R. Cammi, C. Pomelli, J.W. Ochterski, P.Y. Ayala, K. Morokuma, G.A. Voth, P. Salvador, J.J. Dannenberg, V.G. Zakrzewski, S. Dapprich, A.D. Daniels, M.C. Strain, O. Farkas, D.K. Malick, A.D. Rabuck, K. Raghavachari, J.B. Foresman, J.V. Ortiz, Q. Cui, A.G. Baboul, S. Clifford, J. Cioslowski, B.B. Stefanov, G. Liu, A. Liashenko, P. Piskorz, I. Komaromi, R.L. Martin, D.J. Fox, T. Keith, M.A. Al-Laham, C.Y. Peng, A. Nanayakkara, M. Challacombe, P.M.W. Gill, B. Johnson, W. Chen, M.W. Wong, C. Gonzalez and J.A. Pople, Gaussian 03, Wallingford. CT., 2004.
[22] C. Lee, W. Yang, R.G. Parr, Phys. Rev. B: Condens. Matter 37 (1988) 785.
[23] A.D. Becke, J. Chem. Phys. 98 (1993) 5648.
[24] J.P. Perdew, K. Burke, Y. Wang, Phys. Rev. B 54 (1996) 16533.
[25] G.A. Zhurko, Chemcraft, 2010.
[26] N.K. Artemova, V.A. Smirnov, B.G. Rogachev, G.V. Shilov, M. Aldoshin, Russ. Chem. Bull. 55 (2006) 1605.
[27] D.R. Lide, in: C. Press (Ed.), Bond Lengths in Crystalline Organic Compounds, CRC Handbook of Chemistry and Physics, vol. 9, Taylor and Francis, Boca Raton, FL, 2010.
[28] D. Zhang, J. Su, X. Ma, H. Tian, Tetrahedron 64 (2008) 8515.
[29] G. Häfelinger, H.G. Mack, in: Z. Rappoport, S. Patai, (Eds.), The Chemistry of Functional Groups. The Chemistry of Enamines, Enamines: General and Theoretical Aspects, vol. 1. Interscience, Chichester, 1994.
[30] I. André, C. Foces-Foces, F.H. Cano, M. Martínez-Ripoll, Acta Crystallogr. B 53 (1997) 996.
[31] G.R. Desiraju, Acc. Chem. Res. 29 (1996) 441.
[32] J. Bernstein, R.E. Davis, L. Shimoni, C. Ning-Leh, Angew. Chem. Int. Ed. 34 (1995) 1555.
[33] H. Arslan, U. Flörke, N. Külcü, Spectrochim. Acta A 67 (2007) 936.

[34] M. Szafran, P. Barczynski, A. Komasa, Z. Dega-Szafran, J. Mol. Struct. 887 (2008) 20.
[35] A.P. Scott, L. Radom, J. Phys. Chem. 100 (1996) 16502.
[36] M.A. Palafox, Int. J. Quantum Chem. 77 (2000) 661.
[37] M.A. Palafox, V.K. Rastogi, L. Mittal, Int. J. Quantum Chem. 94 (2003) 189.
[38] Z. Rappoport, in: The Chemistry of Functional Groups, Interscience, Chichester, 1994.
[39] R.M. Silverstein, F.X. Webster, D.J. Kiemle, Spectrometric Identification of Organic Compounds, seventh ed., John Wiley & Sons, Inc., Hoboken, NJ, 2005.
[40] B. Osmiałowski, E. Kolehmainen, R. Gawinecki, Magn. Reson. Chem. 39 (2001) 334.
[41] J. Mäki, P. Tähtinen, L. Kronberg, K.D. Klika, J. Phys. Org. Chem. 18 (2005) 240.